Single-scan quantum process tomography

Abhishek Shukla and T. S. Mahesh*

Department of Physics and NMR Research Center, Indian Institute of Science Education and Research, Pune 411008, India

(Received 27 May 2014; revised manuscript received 5 September 2014; published 4 November 2014)

The standard procedure for quantum process tomography (QPT) requires a series of experiments. Each experiment involves initialization of the system to a particular basis state, applying the quantum process ε on the system, and finally characterizing the output state by quantum state tomography (QST). The output states collected for a complete set of basis states enable us to calculate the χ matrix characterizing the process ε. The standard procedure for QST itself requires independent experiments, each involving measurement of a set of commuting observables. Thus QPT procedure demands a number of independent measurements and, moreover, this number increases rapidly with the size of the system. However, in ensemble systems, the total number of independent measurements can be greatly reduced with the availability of ancilla qubits. Ancilla-assisted process tomography (AAPT) has earlier been shown to require a single QST of system-ancilla space. Ancilla-assisted quantum state tomography (AAQST) has also been shown to perform QST in a single-scan measurement of an ensemble system. Here we combine AAPT with AAQST to realize a single-scan QPT (SSPT), a procedure to characterize a general quantum process in a single ensemble measurement. We demonstrate experimental SSPT by characterizing several single-qubit processes using a three-qubit NMR quantum register. Furthermore, using the SSPT procedure, we experimentally characterize the twirling process and compare the results with theory.

DOI: 10.1103/PhysRevA.90.052301 PACS number(s): 03.67.Lx, 03.67.Ac, 03.65.Wj, 03.65.Ta

I. INTRODUCTION

An open quantum system may undergo an evolution due to intentional control fields as well as unintentional interactions with stray fields caused by environmental fluctuations. In practice, even a carefully designed control field may be imperfect to the extent that one might need to characterize the overall process acting on the quantum system. Such a characterization, achieved by a procedure called quantum process tomography (QPT), is crucial in the physical realization of a fault-tolerant quantum processor [1,2]. Quantum process tomography is realized by considering the quantum process as a map from a complete set of initial states to final states and experimentally characterizing each of the final states using quantum state tomography (QST) [3]. Since the spectral decomposition of a density matrix may involve noncommuting observables, Heisenberg's uncertainty principle demands multiple experiments to characterize the quantum state. Thus QST by itself involves the measurement of a series of observables after identical preparations of the system in the quantum state. Hence, QPT in general requires a number of independent experiments, each involving initialization of the quantum system, applying the process to be characterized, and finally QST. Furthermore, the total number of independent measurements required for QPT increases exponentially with the size of the system undergoing the process.

The physical realization of QPT has been demonstrated on various experimental setups such as NMR [4,5], linear optics [6–9], ion traps [10,11], superconducting qubits [12–17], and nitrogen-vacancy center qubit [18]. Several developments in the methodology of QPT have also been reported [19,20]. In particular, it has been shown that ancilla-assisted process tomography (AAPT) can characterize a process with a single QST [6,7,21,22]. However, it still requires multiple measurements, each taken over a set of commuting observables. On the other hand, if sufficient ancilla qubits are available, QST can be carried out with a single ensemble measurement (i.e., a single scan) over the entire system-ancilla space. This procedure, known as ancilla-assisted quantum state tomography (AAQST), has been studied both theoretically and experimentally [23–27]. Here we combine AAPT with AAQST and realize a single-scan quantum process tomography (SSPT), which can characterize a general process in a single ensemble measurement of the system-ancilla state.

In the next section, after briefly revising QPT and AAPT, we describe the SSPT procedure. In Sec. III we illustrate SSPT using a three-qubit NMR quantum register. We characterize certain unitary processes corresponding to standard quantum gates. We also characterize a nonunitary process, namely, twirling operation. Finally, we summarize in Sec. IV.

II. THEORY

A. Quantum process tomography

A process ε maps a quantum state ρ to another state $\varepsilon(\rho)$. Here we consider an n-qubit system with N^2- $(=2^{2n})$ dimensional Liouville space S. In order to characterize ε, we let the process act on each linearly independent element of a complete basis set $\{\rho_1,\rho_2,\ldots,\rho_{N^2}\}$. Expressing each output state in the complete basis, we obtain

$$\varepsilon(\rho_j) = \sum_k \lambda_{jk}\rho_k, \tag{1}$$

where the complex coefficients λ_{jk} can be extracted after QST.

The outcome of a trace-preserving quantum process ε also has an operator-sum representation

$$\varepsilon(\rho) = \sum_i E_i \rho E_i^\dagger, \tag{2}$$

*mahesh.ts@iiserpune.ac.in

where the Kraus operators E_i satisfy the completeness relation $\sum_i E_i^\dagger E_i = \mathbb{1}$. To assist experimental characterization of the process, we utilize a fixed set of basis operators $\{\tilde{E}_m\}$ and express $E_i = \sum_m e_{im}\tilde{E}_m$. The process is now described by

$$\varepsilon(\rho) = \sum_{mn} \tilde{E}_m \rho \tilde{E}_n^\dagger \chi_{mn}, \tag{3}$$

where $\chi_{mn} = \sum_i e_{im} e_{in}^*$ form a complex matrix that completely characterizes the process ε. Since the set $\{\rho_k\}$ forms a complete basis, it is also possible to express

$$\tilde{E}_m \rho_j \tilde{E}_n^\dagger = \sum_k \beta_{jk}^{mn} \rho_k, \tag{4}$$

where β_{jk}^{mn} can be calculated theoretically. Equations (1), (3), and (4) lead to

$$\varepsilon(\rho_j) = \sum_k \lambda_{jk}\rho_k = \sum_k \sum_{mn} \beta_{jk}^{mn} \chi_{mn} \rho_k. \tag{5}$$

Exploiting the linear independence of $\{\rho_k\}$, one obtains the matrix equation

$$\beta\chi = \lambda, \tag{6}$$

from which the χ matrix can be extracted by standard methods in linear algebra.

For example, in the case of a single qubit, one can choose the linearly independent basis $\{|0\rangle\langle 0|, |0\rangle\langle 1|, |1\rangle\langle 0|, |1\rangle\langle 1|\}$ [see Fig. 1(a)]. While the middle two elements are non-Hermitian, they can be realized as a linear combination of Hermitian density operators [28]. A fixed set of operators $\{I, X, -iY, Z\}$ can be used to express the χ matrix. Thus the standard single-qubit QPT procedure requires four QST experiments.

Quantum process tomography on an N-dimensional system requires N^2 QST experiments, where a single QST involves several quantum measurements, each taken jointly over a set of commuting observables. The exact number of measurements required for QST may depend on the properties of available detectors.

In NMR, a single-scan experiment allows us to detect all the single-quantum elements of the density matrix (see Fig. 1). For example, the real NMR signal of a two-qubit system consists of four transitions corresponding to the four observables $\{\sigma_x \otimes |0\rangle\langle 0|, \sigma_x \otimes |1\rangle\langle 1|, |0\rangle\langle 0| \otimes \sigma_x, |1\rangle\langle 1| \otimes \sigma_x\}$. Thus a quadrature detected NMR signal directly provides information about four density-matrix elements [29]. To measure other elements, one needs to transform the density matrix by a known unitary and again record the four transitions. The intensities of these transitions are proportional to linear combinations of various elements of the density matrix. In principle, two experiments suffice for a two-qubit QST [26]. In the case of an n-qubit NMR system with a well-resolved spectrum, QST requires $\simeq \lceil \frac{N}{n} \rfloor$ measurements, where $\lceil \rfloor$ rounds the argument to the next integer [26]. Therefore, n-qubit QPT needs a total of $M_{\rm QPT} \simeq N^2 \lceil \frac{N}{n} \rfloor$ measurements. Estimates of M for a small number of qubits shown in the first column of Table I illustrate the exponential increase of $M_{\rm QPT}$ with n.

B. Ancilla-assisted process tomography

If a sufficient number of ancillary qubits are available, AAPT can be carried out by simultaneously encoding all the basis elements onto a higher-dimensional system-ancilla Liouville space $A \otimes S$ [6,7,21,22]. Ancilla-assisted process tomography requires a single final QST, thus greatly reducing the number of independent measurements. For example, a single-qubit process tomography can be carried out with the help of an ancillary qubit by preparing the two-qubit Bell state $|\phi_{AS}\rangle = (|0_A\rangle|0_S\rangle + |1_A\rangle|1_S\rangle)/\sqrt{2}$, applying the process on the system qubit, and finally carrying out QST of the two-qubit state [see Fig. 1(b)]. While the choice of the initial state for AAPT is not unique, the above choice provides a simple way to represent all the four (2×2)-dimensional basis states directly onto different subspaces of the (4×4)-dimensional density operator [see Figs. 1(a) and 1(b)].

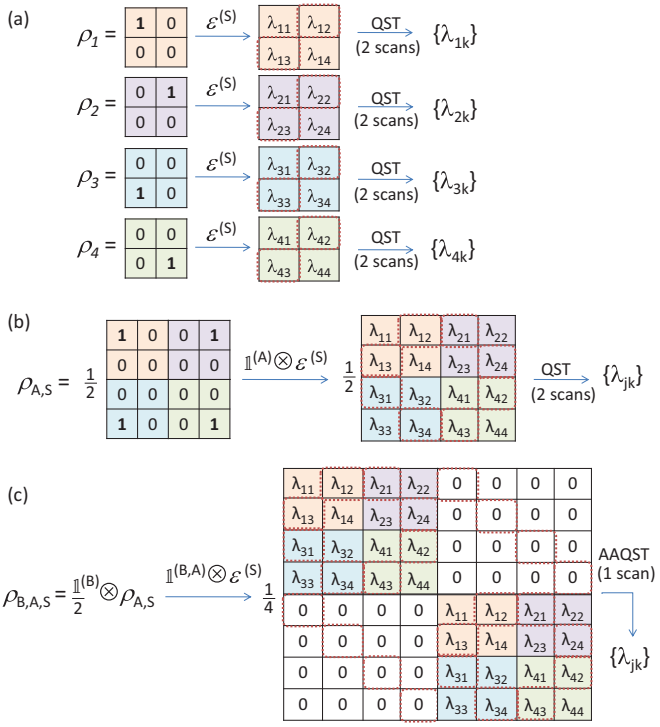

FIG. 1. (Color online) Illustration of (a) single-qubit QPT requiring a total of eight NMR scans, (b) AAPT requiring two NMR scans, and (c) SSPT requiring a single-scan NMR experiment. In each case, dotted lines are used to indicate the single-quantum elements of the density matrix that are directly observable. Other elements are observed by converting them to observable single-quantum coherences by using certain unitary operations in a subsequent scan (or scans).

TABLE I. Comparison of the number of scans and the number of ancilla qubits (in parentheses) required for n-qubit QPT, AAPT, and SSPT.

n	$M_{\rm QPT}$	$M_{\rm AAPT}$	(n_A)	$M_{\rm SSPT}$	(n_A, n_B)
1	8	2	(1)	1	(1,1)
2	32	4	(2)	1	(2,2)
3	192	11	(3)	1	(3,3)
4	1024	32	(4)	1	(4,5)
5	7168	103	(5)	1	(5,6)

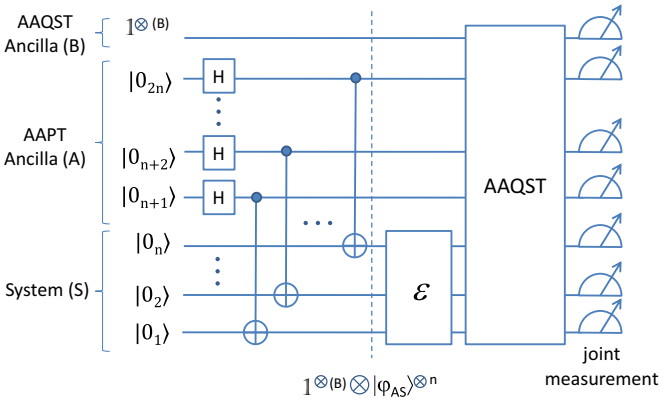

FIG. 2. (Color online) Quantum circuit for SSPT.

For an n-qubit system, all the N^2 basis elements can be encoded simultaneously in independent subspaces of a single $N^2 \times N^2$ Liouville operator belonging to a $2n$-qubit space $A \otimes S$. A simple choice for the initial state is of the form $|\phi_{AS}\rangle^{\otimes n}$. The quantum circuit for the preparation of this state is shown in the first part of Fig. 2. Thus exactly n ancilla qubits are needed to carry out AAPT on an n-qubit system.

Although only two independent measurements are needed for a two-qubit QST, this number grows exponentially with the total number of qubits. An n-qubit AAPT involves a $2n$-qubit QST and accordingly requires $M_{\mathrm{AAPT}} \simeq \lceil \frac{N^2}{2n} \rfloor$ scans [26]. The minimum number of scans for a few system qubits are shown in the second column of Table I. While AAPT requires significantly fewer measurements compared to QPT, it still scales exponentially with the number of system qubits.

C. Single-scan process tomography

It has been shown earlier that, if a sufficient number of ancillary qubits are available, QST of a general density matrix of arbitrary dimension can be performed with a single scan [24–26]. This method, known as ancilla-assisted quantum state tomography, is based on the redistribution of all elements of the system density matrix onto a joint density matrix in the combined system-ancilla Liouville space. Initially the ancilla register for AAQST is prepared in a maximally mixed state, thus erasing all information in it, and redistribution of matrix elements is achieved by an optimized joint unitary operator [26]. By combining AAPT with AAQST, process tomography can be achieved with a single-scan measurement of all the qubits [see Fig. 1(c) and column 3 of Table I]. If AAQST is carried out with an ancilla space B of n_B qubits, the combined space $B \otimes A \otimes S$ corresponds to $\tilde{n} = 2n + n_B$ qubits. A single-scan measurement suffices if the total number of observables is equal to or exceeds the number of real unknowns (i.e., $N^4 - 1$) in the $2n$-qubit density matrix, i.e., if $\tilde{n}\tilde{N} \geqslant N^4 - 1$, where $\tilde{N} = 2^{\tilde{n}}$ [26]. However, if only pairwise interactions are used between the system and ancilla of the same dimension, then also a single experiment suffices for AAQST [27]. The numbers of ancillary qubits n_A and n_B required for SSPT are shown in column 6 of Table I.

The complete circuit for SSPT is shown in Fig. 2. It involves two ancilla registers, one for AAPT and the other for AAQST. Initially the AAQST register is prepared in a maximally mixed state and the other two registers are set to $|0\rangle^{\otimes n}$ states. Hadamard gates on the AAPT ancilla followed by C-NOT gates (on system qubits controlled by the ancilla) prepare the state $|\phi_{AS}\rangle^{\otimes n}$, which simultaneously encodes all the basis elements required for QPT. A single application of the process ε on the system qubits acts simultaneously and independently on all the basis elements $\{\rho_j\}$. The final AAQST operation allows estimation of all the elements of the $2n$-qubit density matrix $\sum_j A^{(j)} \otimes \varepsilon(\rho_j)$, where $A^{(j)}$ identifies the jth subspace. The output of each subspace $\varepsilon(\rho_j)$ can now be extracted using a single-scan experiment and the coefficients $\lambda_{jk} = \mathrm{Tr}[\varepsilon(\rho_j)\rho_k^\dagger]$ can be calculated.

III. EXPERIMENTS

We used iodotrifluoroethylene dissolved in acetone-D_6 as a three-qubit system. The molecular structure and labeling scheme are shown in Fig. 3(a). All the experiments described below are carried out on a Bruker 500-MHz NMR spectrometer at an ambient temperature of 300 K using high-resolution NMR techniques. The NMR Hamiltonian in this case can be expressed as

$$\mathcal{H} = -\pi \sum_{i=1}^{3} \nu_i \sigma_z^i + \pi \sum_{i=1, j>i}^{3,3} J_{ij} \sigma_z^i \sigma_z^j / 2, \qquad (7)$$

where σ_z^i and σ_z^j are Pauli z operators of the ith and jth qubits [29]. The chemical shifts ν_i, coupling constants J_{ij}, and relaxation parameters T_1 and T_2^* are shown in Fig. 3(b). All the pulses are realized using gradient ascent pulse engineering technique [30] and have average fidelities above 0.99 over 20% inhomogeneous rf fields.

We utilize spins F_1, F_2, and F_3, respectively, and the system qubit S, AAPT ancilla A, and AAQST ancilla B. The NMR pulse sequence for SSPT experiments is shown in Fig. 3(c). It begins with preparing the B qubit in the maximally mixed state by bringing its magnetization into the transverse

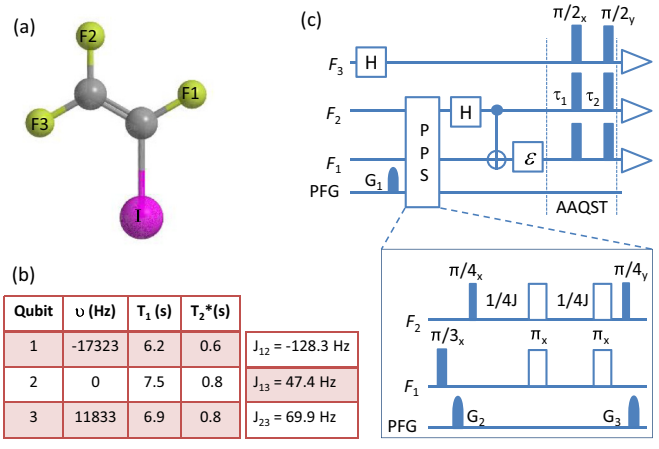

Qubit	υ (Hz)	T_1 (s)	T_2*(s)
1	-17323	6.2	0.6
2	0	7.5	0.8
3	11833	6.9	0.8

J_{12} = -128.3 Hz
J_{13} = 47.4 Hz
J_{23} = 69.9 Hz

FIG. 3. (Color online) (a) Molecular structure of iodotrifluoroethylene, (b) table of Hamiltonian and relaxation parameters, and (c) NMR pulse sequence to demonstrate SSPT. The pulse sequence for preparing the $|00\rangle$ pseudopure state is shown in the inset of (c).

direction using a Hadamard gate and subsequently dephasing it using a pulsed field gradient (PFG). The remaining qubits are initialized into a pseudopure $|00\rangle$ state by applying the standard pulse sequence shown in the inset of Fig. 3(c) [31]. The Bell state $|\phi_{AS}\rangle$ prepared using a Hadamard-CNOT combination has a fidelity of over 0.99. After preparing this state, we apply the process ε to the system qubit. The final AAQST consists of $(\pi/2)_x$ and $(\pi/2)_y$ pulses on all the qubits separated by delays $\tau_1 = 6.7783$ ms and $\tau_2 = 8.0182$ ms [26]. A single-scan measurement of all the qubits now leads to a complex signal of 12 transitions, from which all the 15 real unknowns of the two-qubit density matrix $\rho_{AS} = \sum_j A^{(j)} \otimes \varepsilon(\rho_j)$ of F_1 and F_2 can be estimated [26] (see Fig. 1). In our choice of the fixed set of operators and basis elements

$$\rho_{AS} = \begin{bmatrix} \lambda_{11} & \lambda_{12} & \lambda_{21} & \lambda_{22} \\ \lambda_{13} & \lambda_{14} & \lambda_{23} & \lambda_{24} \\ \lambda_{31} & \lambda_{32} & \lambda_{41} & \lambda_{42} \\ \lambda_{33} & \lambda_{34} & \lambda_{43} & \lambda_{44} \end{bmatrix}. \tag{8}$$

The χ matrix characterizing the complete process can now be obtained by solving Eq. (6).

A. Single-scan process tomography of quantum gates

We now describe experimental characterization of several single-qubit unitary processes. The quantum gates to be characterized are introduced as process ε on the F_1 qubit in Fig. 3(c). The experimental χ matrices for NOP (identity process), NOT-X ($e^{-i\pi X/2}$), NOT-Y ($e^{-i\pi Y/2}$), the Hadamard gate, phase π ($e^{i\pi Z/2}$), and phase $\pi/4$ ($e^{i\pi Z/8}$) are shown in Fig. 4. Starting from thermal equilibrium, each SSPT experiment characterizing an entire one-qubit process takes less than 4 s. A measure of overlap of the experimental process χ_{expt} with the theoretically expected process χ_{theor} is given by the gate fidelity [18]

$$F(\chi_{\text{expt}}, \chi_{\text{theor}}) = \frac{|\text{Tr}[\chi_{\text{expt}} \chi^\dagger_{\text{theor}}]|}{\sqrt{\text{Tr}[\chi^\dagger_{\text{expt}} \chi_{\text{expt}}]\text{Tr}[\chi^\dagger_{\text{theor}} \chi_{\text{theor}}]}}. \tag{9}$$

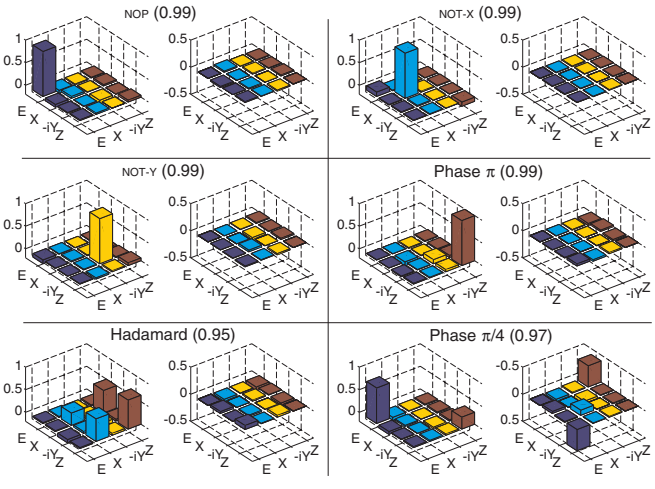

FIG. 4. (Color online) Bar plots showing experimental χ matrices for various quantum processes obtained using SSPT. In each case, the left and right bar plots correspond to the real and imaginary parts, respectively, and the fidelities are indicated in parentheses.

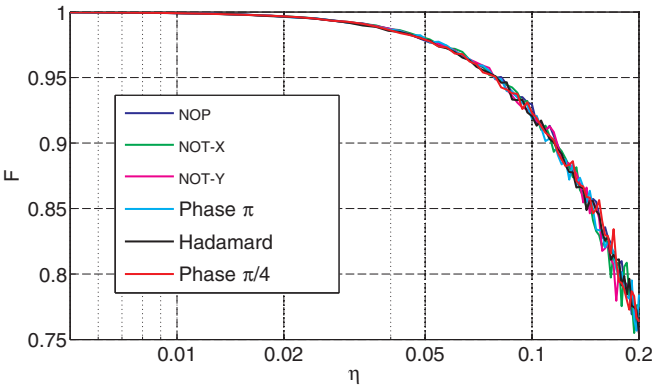

FIG. 5. (Color online) Simulated fidelity of various processes as a function of noise η.

The gate fidelities for all six processes are indicated in Fig. 4. Except in the cases of the Hadamard gate and phase $\pi/4$, the gate fidelities are about 0.99. The lower fidelities in the Hadamard gate (0.95) and phase $\pi/4$ (0.97) are mainly due to imperfections in the rf pulses implementing these processes.

In order to study the robustness of SSPT procedure we first considered an ideal process, simulated the corresponding spectral intensities, and reconstructed the final density matrix ρ_{AS}. Using Eq. (8) we obtained λ_{jk} values and calculated the matrix χ_0 simulating the noise-free SSPT procedure. We then introduced noise by adding random numbers in the range $[-\eta, \eta]$ to the spectral intensities and used the resulting data for calculating χ_η. The variations of average gate fidelities $F(\chi_0, \chi_\eta)$ for various processes versus noise amplitude η are shown in Fig. 5. Interestingly, the noise has similar effects on fidelities of all the simulated processes. We also observe that fidelities remained above 0.9 for $\eta < 0.1$, indicating that SSPT is fairly robust against the noise in this range.

B. Single-scan process tomography of twirling process

Twirling is essentially a nonunitary process usually realized by an ensemble average of a set of unitary operations. It was introduced by Bennett *et al.* [32] for extracting singlet states from a mixture of Bell states. Twirling has been studied in detail [33–37] and various modified twirling protocols have also been suggested [38,39].

In NMR, twirling can be achieved with the help of a PFG, which produces a continuous space-dependent spin rotation such that the ensemble average effectively emulates a nonunitary process [40]. A $\hat{z}$ PFG produces a z-dependent unitary $U_\phi(z) = \exp(-i\frac{\phi}{2}\sum_{j=1}^{n}\sigma_{jz})$, where j is the summation index over all the qubits. Assuming a linear gradient introducing a maximum phase $\pm\Phi$ on either end of a sample of length z_0, we have $\phi(z) = 2\Phi(z/z_0)$. When the $\hat{z}$ PFG acts on an initial n-qubit density matrix $\rho_{\text{in}} = \sum_{lm}\rho_{lm}|l\rangle\langle m|$, the resultant output density matrix is

$$\rho_{\text{out}} = \frac{1}{2\Phi}\int_{-\Phi}^{\Phi} d\phi\, U_\phi \rho_{\text{in}} U_\phi^\dagger = \sum_{lm}\rho_{lm}|l\rangle\langle m|\text{sinc}(q_{lm}\Phi). \tag{10}$$

Here $\text{sinc}(x) = \frac{\sin x}{x}$ and $q_{lm} = \frac{1}{2}\sum_j[(-1)^{m_j} - (-1)^{n_j}]$ is the quantum number of the element $|l_1 l_2 \cdots l_n\rangle\langle m_1 m_2 \cdots m_n|$,

i.e., the difference in the spin-quantum numbers of the corresponding basis states. While the diagonal elements $|l\rangle\langle l|$ and other zero-quantum elements are unaffected by twirling, the off-diagonal elements with $q_{lm} \neq 0$ undergo decaying oscillations with increasing Φ values.

Single-scan process tomography of twirling process is carried out using the procedure described in Fig. 3(c) after introducing δ-PFG-δ in place of the process ε, where δ is a short delay for switching the gradient. Applying PFG selectively on the system qubit is not simple and is also unnecessary. Since the F_3 qubit (AAQST ancilla) is already in a maximally mixed state, twirling has no effect on it. For the Bell state $|\phi_{AS}\rangle$, applying a strong twirling on either or both spins (F_1, F_2) has the same effect, i.e., a strong measurement reducing the joint state to a maximally mixed state. However, since $|\phi_{AS}\rangle$ corresponds to a two-quantum coherence (i.e., $q_{00,11} = 2$), its dephasing is double that of a single-quantum coherence. Assuming the initial state $\rho_{\rm in} = |\phi_{AS}\rangle\langle\phi_{AS}|$ and using expressions (1) and (10), we find that the nonzero elements of λ are

$$\lambda_{11} = \lambda_{44} = 1, \quad \lambda_{22} = \lambda_{33} = \mathrm{sinc}(2\Phi). \tag{11}$$

Solving expression (6), we obtain a real χ matrix with only nonzero elements

$$\chi_{\rm EE} = \frac{1 + \mathrm{sinc}(2\Phi)}{2}, \quad \chi_{\rm ZZ} = \frac{1 - \mathrm{sinc}(2\Phi)}{2}. \tag{12}$$

In our experiments, the duration of the PFG and δ are set to 300 and 52.05 μs, respectively, such that the chemical shift evolutions and J evolutions are negligible. The strength of twirling is slowly varied by increasing the PFG strength from 0 to 2.4 G/cm in steps of 0.05 G/cm. The results of the experiments are shown in Fig. 6. The closed squares (circles) in Fig. 6(a) correspond to experimentally obtained values for $|\chi_{\rm EE}|$ ($|\chi_{\rm ZZ}|$). Small imaginary parts observed in experimental χ matrices are due to minor experimental imperfections. The smooth lines indicate the corresponding theoretical values obtained from Eqs. (12). The crosses indicate the gate fidelities $F(\chi_{\rm expt}, \chi_{\rm theor})$ calculated using Eq. (9). The bar plots show

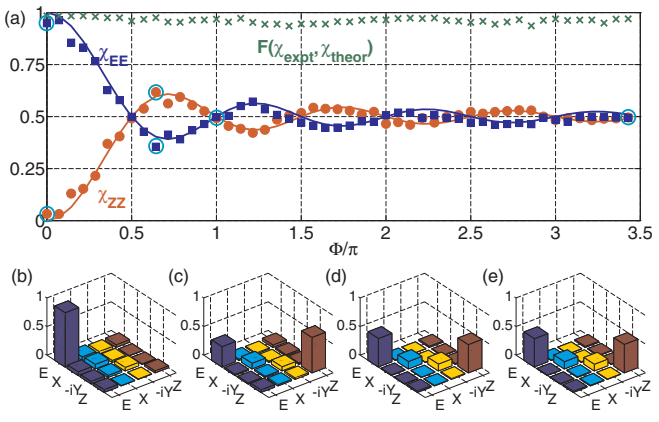

FIG. 6. (Color online) (a) Experimental values of $|\chi_{\rm EE}|$ ($|\chi_{\rm ZZ}|$) shown by closed squares (closed circles). The solid lines illustrate theoretical values of $\chi_{\rm EE}$ and $\chi_{\rm ZZ}$. The crosses indicate the gate fidelities $F(\chi_{\rm expt}, \chi_{\rm theor})$. The bar plots correspond to experimental $|\chi|$ matrices at (b) $\Phi = 0$, (c) $\Phi = 0.64\pi$, (d) $\Phi = \pi$, and (e) $\Phi = 3.43\pi$.

experimental $|\chi|$ matrices for $\Phi = 0$ [Fig. 6(b)], $\Phi = 0.64\pi$ [Fig. 6(c)], $\Phi = \pi$ [Fig. 6(d)], and $\Phi = 3.43\pi$ [Fig. 6(e)] and $\chi_{\rm EE}$ and $\chi_{\rm ZZ}$ values in Fig. 6(a) corresponding to these Φ values are circled out.

At zero twirling, the process is essentially a NOP process as is clear from the bar plot in Fig. 6(b), wherein $|\chi_{\rm EE}| \approx 1$ and $|\chi_{\rm ZZ}| \approx 0$. When $\Phi = k\pi/2$ with an integer k, the ensemble initially prepared in state $|\psi_{AS}\rangle$ undergoes an overall phase distribution over $[-k\pi, k\pi]$ and at this stage $\chi_{\rm EE} = \chi_{\rm ZZ} = 0.5$ [see, e.g., Fig. 6(d)]. A further increase in Φ leads to oscillations of $\chi_{\rm EE}$ and $\chi_{\rm ZZ}$ about 0.5 and for large Φ values both of these elements damp towards 0.5 and all other elements vanish [see, e.g., Fig. 6(e)]. The errors in experimental $\chi_{\rm EE}$ and $\chi_{\rm ZZ}$ values were less than 8%. The good agreement of the experimental values with theory indicates the overall success of the SSPT procedure. The average of the gate fidelities was over 0.96. Small deviations of the experimental values from theory are due to nonlinearities in the PFG profile as well as imperfections in rf pulses implementing the SSPT procedure.

IV. CONCLUSION

Information processing requires two important physical resources, namely, the size of the register (space) and the number of operations (time). Often there exists an equivalence between these two resources that allows trading one resource with another. Likewise, in the present work we showed that, if some extra qubits are available, it is possible to carry out quantum process tomography of the system qubits with a single-scan ensemble measurement. We have illustrated this method on a single system qubit and two ancillary qubits using NMR quantum computing methods. In particular, we extracted the χ matrices characterizing certain quantum gates and obtained their gate fidelities with the help of a single ensemble measurement of a three-qubit system in each case. We studied the robustness of the SSPT procedure using numerical simulations. We also characterized the twirling operation, which is essentially a nonunitary process.

The ensemble nature of NMR systems allows us to determine all the single-quantum observables in a single-scan experiment. However, a larger ancilla may be required if measurement of only a commuting set of observables is allowed in a single experiment, as in the case of single-apparatus QST [23] or if the system-ancilla interactions are constrained, as in the pairwise interaction case [27]. Nevertheless, the overall procedure of SSPT can be generalized to apply in other fields such as optical qubits, trapped ions, or superconducting qubits.

A potential application of single-scan process tomography could be in the high throughput characterization of dynamic processes. The standard methods require repeated applications of the same process either to collect independent outputs from all the basis states or to allow quantum state tomography. However, the present method requires only one application of the process for the entire characterization.

ACKNOWLEDGMENTS

The authors are grateful to Professor Anil Kumar, Swathi Hegde, Hemant Katiyar, and Rama Koteswara Rao for discussions. This work was partly supported by DST Project No. SR/S2/LOP-0017/2009.

[1] I. L. Chuang and M. A. Nielsen, J. Mod. Opt. **44**, 2455 (1997).
[2] J. F. Poyatos, J. I. Cirac, and P. Zoller, Phys. Rev. Lett. **78**, 390 (1997).
[3] I. L. Chuang, N. Gershenfeld, M. G. Kubinec, and D. W. Leung, Proc. R. Soc. London Ser. A **454**, 447 (1998).
[4] A. M. Childs, I. L. Chuang, and D. W. Leung, Phys. Rev. A **64**, 012314 (2001).
[5] Y. S. Weinstein, T. F. Havel, J. Emerson, N. Boulant, M. Saraceno, S. Lloyd, and D. G. Cory, J. Chem. Phys. **121**, 6117 (2004).
[6] F. De Martini, A. Mazzei, M. Ricci, and G. M. D'Ariano, Phys. Rev. A **67**, 062307 (2003).
[7] J. B. Altepeter, D. Branning, E. Jeffrey, T. C. Wei, P. G. Kwiat, R. T. Thew, J. L. O'Brien, M. A. Nielsen, and A. G. White, Phys. Rev. Lett. **90**, 193601 (2003).
[8] J. L. O'Brien, G. J. Pryde, A. Gilchrist, D. F. V. James, N. K. Langford, T. C. Ralph, and A. G. White, Phys. Rev. Lett. **93**, 080502 (2004).
[9] M. W. Mitchell, C. W. Ellenor, S. Schneider, and A. M. Steinberg, Phys. Rev. Lett. **91**, 120402 (2003).
[10] M. Riebe, K. Kim, P. Schindler, T. Monz, P. O. Schmidt, T. K. Körber, W. Hänsel, H. Häffner, C. F. Roos, and R. Blatt, Phys. Rev. Lett. **97**, 220407 (2006).
[11] D. Hanneke, J. P. Home, J. D. Jost, J. M. Amini, D. Leibfried, and D. J. Wineland, Nat. Phys. **6**, 13 (2010).
[12] M. Neeley, M. Ansmann, R. C. Bialczak, M. Hofheinz, N. Katz, E. Lucero, A. O'Connell, H. Wang, A. N. Cleland, and J. M. Martinis, Nat. Phys. **4**, 523 (2008).
[13] J. M. Chow, J. M. Gambetta, L. Tornberg, J. Koch, L. S. Bishop, A. A. Houck, B. R. Johnson, L. Frunzio, S. M. Girvin, and R. J. Schoelkopf, Phys. Rev. Lett. **102**, 090502 (2009).
[14] R. C. Bialczak, M. Ansmann, M. Hofheinz, E. Lucero, M. Neeley, A. D. O'Connell, D. Sank, H. Wang, J. Wenner, M. Steffen, A. N. Cleland, and J. M. Martinis, Nat. Phys. **6**, 409 (2010).
[15] T. Yamamoto, M. Neeley, E. Lucero, R. C. Bialczak, J. Kelly, M. Lenander, M. Mariantoni, A. D. O'Connell, D. Sank, H. Wang, M. Weides, J. Wenner, Y. Yin, A. N. Cleland, and J. M. Martinis, Phys. Rev. B **82**, 184515 (2010).
[16] J. M. Chow, A. D. Córcoles, J. M. Gambetta, C. Rigetti, B. R. Johnson, J. A. Smolin, J. R. Rozen, G. A. Keefe, M. B. Rothwell, M. B. Ketchen, and M. Steffen, Phys. Rev. Lett. **107**, 080502 (2011).
[17] A. Dewes, F. R. Ong, V. Schmitt, R. Lauro, N. Boulant, P. Bertet, D. Vion, and D. Esteve, Phys. Rev. Lett. **108**, 057002 (2012).
[18] J. Zhang, A. M. Souza, F. D. Brandao, and D. Suter, Phys. Rev. Lett. **112**, 050502 (2014).
[19] A. Shabani, R. L. Kosut, M. Mohseni, H. Rabitz, M. A. Broome, M. P. Almeida, A. Fedrizzi, and A. G. White, Phys. Rev. Lett. **106**, 100401 (2011).
[20] Z. Wu, S. Li, W. Zheng, X. Peng, and M. Feng, J. Chem. Phys. **138**, 024318 (2013).
[21] A. Mazzei, M. Ricci, F. De Martini, and G. D'Ariano, Fortschr. Phys. **51**, 342 (2003).
[22] G. M. D'Ariano and P. Lo Presti, Phys. Rev. Lett. **91**, 047902 (2003).
[23] A. E. Allahverdyan, R. Balian, and T. M. Nieuwenhuizen, Phys. Rev. Lett. **92**, 120402 (2004).
[24] X. Peng, J. Du, and D. Suter, Phys. Rev. A **76**, 042117 (2007).
[25] Y. Yu, H. Wen, H. Li, and X. Peng, Phys. Rev. A **83**, 032318 (2011).
[26] A. Shukla, K. R. K. Rao, and T. S. Mahesh, Phys. Rev. A **87**, 062317 (2013).
[27] H. Wang, W. Zheng, Y. Yu, M. Jiang, X. Peng, and J. Du, Phys. Rev. A **89**, 032103 (2014).
[28] Nielsen and I. L. Chuang, *Quantum Computation and Quantum Information* (Cambridge University Press, Cambridge, 2010).
[29] J. Cavanagh, W. J. Fairbrother, A. G. Palmer III, and N. J. Skelton, *Protein NMR Spectroscopy: Principles and Practice* (Academic, New York, 1995).
[30] N. Khaneja, T. Reiss, C. Kehlet, T. Schulte-Herbrüggen, and S. J. Glaser, J. Magn. Reson. **172**, 296 (2005).
[31] D. G. Cory, A. F. Fahmy, and T. F. Havel, Proc. Natl. Acad. Sci. USA **94**, 1634 (1997).
[32] C. H. Bennett, G. Brassard, S. Popescu, B. Schumacher, J. A. Smolin, and W. K. Wootters, Phys. Rev. Lett. **76**, 722 (1996).
[33] C. H. Bennett, D. P. DiVincenzo, J. A. Smolin, and W. K. Wootters, Phys. Rev. A **54**, 3824 (1996).
[34] J. Emerson, R. Alicki, and K. Zyczkowski, J. Opt. B **7**, S347 (2005).
[35] J. Emerson, M. Silva, O. Moussa, C. Ryan, M. Laforest, J. Baugh, D. G. Cory, and R. Laflamme, Science **317**, 1893 (2007).
[36] M. Silva, E. Magesan, D. W. Kribs, and J. Emerson, Phys. Rev. A **78**, 012347 (2008).
[37] C. C. López, A. Bendersky, J. P. Paz, and D. G. Cory, Phys. Rev. A **81**, 062113 (2010).
[38] C. Dankert, R. Cleve, J. Emerson, and E. Livine, Phys. Rev. A **80**, 012304 (2009).
[39] O. Moussa, M. P. da Silva, C. A. Ryan, and R. Laflamme, Phys. Rev. Lett. **109**, 070504 (2012).
[40] M. S. Anwar, L. Xiao, A. J. Short, J. A. Jones, D. Blazina, S. B. Duckett, and H. A. Carteret, Phys. Rev. A **71**, 032327 (2005).